IEEE Access
Multidisciplinary | Rapid Review | Open Access Journal

Received December 13, 2020, accepted December 29, 2020, date of publication January 1, 2021, date of current version January 12, 2021.

Digital Object Identifier 10.1109/ACCESS.2020.3048882

Effective Rate Evaluation of RIS-Assisted Communications Using the Sums of Cascaded α-μ Random Variates

LONG KONG [1], YUN AI [2], (Member, IEEE), SYMEON CHATZINOTAS [1], (Senior Member, IEEE), AND BJÖRN OTTERSTEN [1], (Fellow, IEEE)

[1]Interdisciplinary Center for Security, Reliability and Trust (SnT), University of Luxembourg, 1855 Luxembourg City, Luxembourg
[2]Faculty of Engineering, Norwegian University of Science and Technology, 2815 Gjøvik, Norway

Corresponding author: Long Kong (long.kong@uni.lu)

This work was supported in part by the Luxembourg National Research Fund (FNR) projects, titled Exploiting Interference for Physical Layer Security in 5G Networks (CIPHY) under Grant FNR11607830, and in part by the Reconfigurable Intelligent Surfaces for Smart Cities (RISOTTI).

ABSTRACT This paper begins with the characterization of the sum of M versions of cascaded α-μ (equivalently, $N * (\alpha$-$\mu)$) distributed random variates (RVs), and later on, explores the feasibility and applicability of the obtained results in the recent proposed reconfigurable intelligent surface (RIS)-assisted communications. More specifically, the sum of cascaded α-μ distributed RVs is exactly characterized by the probability density function (PDF) expressed in terms of the programmable multivariate Fox's H-function, and approximated with the mixture of Gaussian (MoG) distribution. The approximation accuracy is further validated by the Kolmogorov-Smirnov (KS) goodness of fit test. Based on the obtained statistical results, a promising application, i.e., RIS-assisted communication, is considered and evaluated from the effective rate perspective. The exact, asymptotic, and approximated effective rate are derived with closed-form expressions. Finally, our analytical results are further validated using the Monte-Carlo simulation, their accuracy is confirmed with the analytical error indicator. One can conclude that (i) the exact effective rate expression is complex in the manner of mathematical representation; (ii) the MoG-based effective rate expression is simple and provides a highly tight approximation to the exact expression, besides it indeed acts as a highly tight upper bound for the exact effective rate expression; and (iii) the MoG-based solution outperforms the multivariate Fox's H-function based approach with reducing complexity.

INDEX TERMS Effective rate, quality-of-service (QoS), cascaded α-μ, reconfigurable intelligent surfaces (RIS), Kolmogorov-Smirnov (KS) goodness of fit test, Fox's H-function, mixture of Gaussian (MoG).

I. INTRODUCTION

Future generation of communication systems are bound to change the landscape of industry thanks to the Industrial Internet of Things (IIoT) enabled by extreme low latency and massive number of connections. Due to the highly time-varying characteristics of the wireless channel, deterministic delay constraints are normally difficult to meet. Instead, the statistical quality-of-service (QoS) provisioning turns out to be a useful instrument to evaluate the delay bound QoS guarantees for realistic wireless real-time traffic.

The associate editor coordinating the review of this manuscript and approving it for publication was Jiayi Zhang.

The effective rate serves a statistical QoS metric defined as the maximum constant arrival rate that a time-varying service process can support with statistical latency guarantees [1]–[3]. It acts as a joint mathematical framework, connecting physical layer and link layer, and is used to explore the performance of various wireless networks under certain delay constraint [3]. The concept of effective rate has been widely applied over the last few years to investigate the trade-off among latency, reliability, energy efficiency, and security. Examples can be found in [3], especially in some traditional and future promising applications, including Cellular communication, device-to-device (D2D) communications, peer-to-peer video streaming, visible light

This work is licensed under a Creative Commons Attribution 4.0 License. For more information, see https://creativecommons.org/licenses/by/4.0/

communication, full-duplex communications, non-orthogonal multiple access (NOMA) [4]–[7], vehicle communications [8], and ultra-reliable low latency communications (URLLC).

A. BACKGROUND AND RELATED WORKS

The effective rate investigation of these applications are conducted under different fading channel models. The effective rate metric of various small-scale (or multipath), large-scale (or shadowing), and composite fading channels was widely examined, including Weibull [9], α-μ [10] (equivalently, generalized gamma), κ-μ [11], generalized-$\mathcal{K}$ [12], [13], Fisher-Snedecor $\mathcal{F}$ [14], α-η-μ/Gamma [15], two-wave with diffuse-power (TWDP) [16], double shadowed Rician [17], α-η-κ-μ[1] [18], [19], κ-μ/inverse gamma and η-μ/inverse gamma [20], etc. In [21], the authors investigated the effective rate of multiple-input multiple-output (MIMO) keyhole channels (i.e., rank one MIMO channel). Rare efforts have ever been seen about the investigation for the analytical analysis of effective rate over cascaded fading channels.

B. MOTIVATIONS

To this end, the focus of this paper lies in the investigation of the effective rate analysis over cascaded fading models. It is worth mentioning that the cascaded fading models can capably represent a mobile-to-mobile (M2M) scenario both through analysis and measurement [22]. The cascaded fading models can be physically interpreted as follows: the received signals are generated by the product of a large number of rays reflected via N statistically independent scatters [23]–[25]. Those models are applicable for the multi-hop non-regenerative amplify-and-forward (AF) relaying system with fixed gain [26], the propagation in the presence of keyholes, the keyhole phenomena in MIMO systems [21], and reconfigurable intelligent surfaces (RIS)-assisted wireless system [27]. An RIS, in other words, is also equivalent to digitally controllable scatters and software-defined surface [28]. The large number of small, low-cost, and passive artificial 'meta-atoms' embedded in an RIS are able to smartly change the reflection direction towards any desired users by tuning a series of phase shifters [29], [30]. More specifically, the authors of [29], [30] explored the feasibility of applying the RIS technology to the future sixth-generation (6G) and beyond fifth-generation (5G) networks from the viewpoints of modulation and multiple antenna, respectively.

In [24], the authors proposed a flexible and general 'multiplicative' stochastic model, namely, the cascaded α-μ ($N * (\alpha$-$\mu)$) fading channel. It is flexible and mathematical tractable, since it can elaborate the cascaded Rayleigh, Nakagami-m [23], exponential, Gamma, Weibull, and lognormal ($\alpha \to \infty, \mu \to \infty$) fading by simply attributing the fading parameters α and μ to selected values. For instance, setting $\alpha = 2$ and $\mu = 1$, it will reduce to cascaded Rayleigh fading, whereas choosing $\alpha = 2$ and $\mu = m$ will make it correspond to cascaded Nakagami-m fading. More importantly, the α-μ distribution was proposed by Yacoub in [31] to model the small-scale variation of fading signal under line-of-sight conditions [32], [33]. It is physically described with two key fading parameters, i.e., nonlinearity of the propagation medium α and the clustering of the multipath waves μ. The advantage of these two factors is regarded as a useful tool to vividly depict the inhomogeneous surroundings compared with other existing fading models, such as Rayleigh and Nakagami-m. Most of these are based on the assumption of a rarely-encountered scenario of homogeneous (scattering) environment. Fortunately, the α-μ fading model was later on found valid and feasible in many realistic situations [34]–[39], including the vehicle-to-vehicle (V2V) communication networks and wireless body area networks (WBAN).

Moreover, the sum of α-μ distributed random variates (RVs) has been investigated in [40], where a new α-μ distributed RV is used to highly approximate the sum. Similarly, the sums of other general fading models, e.g., η-μ, κ-μ, Fisher-Snedecor $\mathcal{F}$, fluctuating two-ray (FTR), and Fox's H-function distributed RVs are also characterized in [41]–[47], where their application to the maximal-ratio-combining (MRC) diversity receiver are correspondingly investigated with the assistance of the obtained statistical results [42]–[47].

To this end, the core of interest in this paper is to characterize the sum of cascaded α-μ RVs. Different from the MRC diversity receivers, in this paper we consider the newly proposed RIS-assisted communications as a possible and promising application based on the obtained statistical results. In continuation with the aforementioned discussion about the effective rate analysis, the usefulness of our findings is further evaluated from the effective rate perspective.

C. CONTRIBUTIONS AND ORGANIZATION

The main contributions of this paper are summarized as follows:

1) Characterizing the probability density function (PDF) for the sum of M version of cascaded $\alpha - \mu$ distributed RVs, which is expressed in terms of the multivariate Fox's H-function. For the purpose of providing a reducing complexity solution, the sum of cascaded α-μ RVs is also modeled in the manner of the mixture of Gaussian (MoG) distribution, the approximation accuracy is further confirmed using the Kolmogorov-Smirnov (KS) goodness of fit test.
2) Initially applying the sum of cascaded distributed RVs to the novel RIS-assisted communication, and exploring the feasibility and advantages of using the obtained statistical result to the RIS-assisted communications from the effective rate perspective.
3) Deriving the exact, asymptotic, and approximated effective rate expressions of the RIS-aided

[1] As shown in [18], the α-η-κ-μ distribution includes the α-μ, κ-μ, and η-μ distributions as its special cases.

communications over α-μ fading channels. Especially when $M = 1$, the exact effective rate analysis fills the gap of lacking effective rate analysis over cascaded fading channels.

4) Validating the accuracy and tightness of the exact and asymptotic behavior of the analytical results with Monte-Carlo simulations.
5) Providing the asymptotic effective rate slope at high signal-to-noise ratio (SNR) regime.
6) One can surely conclude that (i) the exact, asymptotic, and approximated effective rate expressions are analytically correct; (ii) the RIS-aided communications is a suitable application of the sum of cascaded α-μ distributed RVs, and the increase of M leads to an enhancement of the overall effective rate; and iii) the MoG-based approach is quite advantageous since it provides a simple and easy solution to analyze the effective rate over various wireless fading channels with reducing complexity.

The rest of this paper is organized as follows: Section II provides the preliminary results regarding the sum of cascaded α-μ distributed RVs. Based on the obtained results, we present a system configuration of the RIS-assisted communications in Section III. Next, the exact, asymptotic, and approximated effective rate expressions of our proposed system model are subsequently analyzed in Section IV. Section V demonstrates the numerical results and some interesting discussions. Finally, Section VI concludes this paper.

Mathematical Functions and Notations: $w = \sqrt{-1}$, $f_X(x)$ represents the probability density function (PDF) of RV X, $H_{p,q}^{m,n}[\cdot]$ is the univariate Fox's H-function [48, Eq. (1.2)], $\Gamma(\cdot)$ denotes the gamma function. $H_{p,q;p_1,q_1;\cdots;p_L,q_L}^{m,n;m_1,n_1;\cdots;m_L,n_L}[\cdot]$ is the multivariate Fox's H-function [48, A.1]. $\mathrm{erf}(\cdot)$ is the error function. $G_{p,q}^{m,n}[\cdot]$ is the Meijer's G-function and it is a special case of Fox's H-function [48, Eq. (1.111)]. $\mathbb{E}(x)$ is the expectation operator over an RV x. $\mathrm{Res}[f(x), s]$ represents the residue of function $f(x)$ at pole $x = s$.

II. PRELIMINARY

A. CHARACTERIZATION OF THE SUM OF CASCADED α-μ RVs

Let $\mathcal{Z}$ be the product of $N, N \geq 1$, independently α-μ distributed RVs having parameters (α_i, μ_i), i.e., $\mathcal{Z} = \prod_{i=1}^{N} z_i$, the PDF of z_i is given by [31]

$$f_{z_i}(x) = \frac{\alpha_i \mu_i^{\mu_i} x^{\alpha_i \mu_i - 1}}{\Omega_i^{\alpha_i \mu_i} \Gamma(\mu_i)} \exp\left(- \mu_i \left(\frac{x}{\Omega_i} \right)^{\alpha_i} \right) \overset{(a)}{=} \kappa_i H_{0,1}^{1,0}\left[\lambda_i x \middle| \begin{matrix} - \\ (\mu_i - \frac{1}{\alpha_i}, \frac{1}{\alpha_i}) \end{matrix} \right], \tag{1}$$

where $\kappa_i = \frac{\mu_i^{\frac{1}{\alpha_i}}}{\Omega_i \Gamma(\mu_i)}$, $\lambda_i = \frac{\mu_i^{\frac{1}{\alpha_i}}}{\Omega_i}$, $\Omega_i = \frac{\Gamma(\mu_i)}{\Gamma\left(\mu_i + \frac{1}{\alpha_i}\right)}$, $i = 1, \cdots, N$. Step (a) holds by using [48, Eq. (1.125)]. The PDF of $\mathcal{Z}$ is thereafter given by [24]

$$f_{\mathcal{Z}}(z) = \mathcal{K}_N H_{0,N}^{N,0}\left[\mathcal{C}_N z \middle| \begin{matrix} - \\ \Phi_1, \cdots, \Phi_N \end{matrix} \right], \tag{2}$$

where $\mathcal{K}_N = \prod_{i=1}^{N} \kappa_i$, $\mathcal{C}_N = \prod_{i=1}^{N} \lambda_i$, $\Phi_i = \left(\mu_i - \frac{1}{\alpha_i}, \frac{1}{\alpha_i}\right)$. For simplicity, let $\mathcal{B} = (\Phi_1, \cdots, \Phi_N)$. As a result, $\mathcal{Z}$ is also called a cascaded α-μ distributed RV.

Apparently, the cascaded α-μ distribution is a special case of the Fox's H-function distribution. To this end, applying the results obtained in [47, Eq. (7)], the PDF of the sum of independent but not identically distributed (i.n.i.d.) cascaded α-μ distributed RVs, i.e., $\mathsf{Z} = \sum_{j=1}^{M} \mathcal{Z}_j$, is given in terms of the multivariate Fox's H-function,[2] i.e.,

$$\begin{aligned} f_{\mathsf{Z}}(z) &= \frac{\eta_M}{z} H\left(\begin{matrix} \binom{0,0}{0,1} \\ \binom{N_j, 1}{1, N_j}_{j=1:M} \end{matrix} \middle| \begin{matrix} - \\ (1; 1_M) \\ \left[(1,1) \right]_{j=1:M} \\ \mathscr{B} \end{matrix} \middle| \left(\mathcal{C}_{N,j} z\right)_{j=1:M} \right) \\ &\overset{(b)}{=} \frac{\eta_M}{(2\pi w)^M z} \int_{\mathcal{L}_1} \cdots \int_{\mathcal{L}_M} \Phi(s_1, \cdots, s_M) \\ &\quad \times \prod_{j=1}^{M} \phi(s_j) (\mathcal{C}_j z)^{s_j} ds_1, \cdots, ds_M, \end{aligned} \tag{3}$$

where $\eta_M = \prod_{j=1}^{M} \frac{\mathcal{K}_{N,j}}{\mathcal{C}_{N,j}}$, $\varphi_i = \left(\mu_i, \frac{1}{\alpha_i}\right)$, $\mathscr{B} = (\varphi_1, \cdots, \varphi_N)$, and $\mathcal{L}_j$ is the integral path from $\delta_j - w\infty$ to $\delta_j + w\infty$, $\Phi(s_1, \cdots, s_M) = \Gamma(\sum_{j=1}^{M} s_j)$, and $\phi(s_j) = \prod_{i=1}^{N} \Gamma\left(\mu_i - \frac{s_j}{\alpha_i}\right) \Gamma(s_j)$. Step (b) is developed for the sake of assisting the asymptotic effective rate analysis.

Note that the multivariate Fox's H-function is feasible and beneficial when analyzing the physical layer security [49], symbol error rate, and channel capacity over Fox's H-function fading channels [50].

As we can see from (3), the PDF is expressed in terms of the multivariate Fox's H-function. In order to provide an easy and straightforward PDF expression, we have in this section investigated the feasibility of re-modeling $\mathsf{Z} = \sum_{j=1}^{M} \mathcal{Z}_j$ with the aid of the MoG distribution. The contribution established in [51] showcased that the MoG distribution can be used to model any arbitrarily shaped non-Gaussian density, e.g., Nakagami/Lognormal, Weibull, κ-μ, η-μ, α-μ distributions, etc. The intrinsic parameters used to represent the MoG distribution are implemented via the completely unsupervised expectation-maximization (EM) learning algorithm. In [52], the MoG distribution is proved extremely advantageous to provide an easy and simple solution when analyzing the physical layer security performance over various fading channels. Motivated by the promising outcomes obtained in [51], [52],

[2] Due to the limited space and for brevity of notations, the multivariate Fox's H-function is presented in the manner of the one given in [47]. 1_N denotes the N-dimensional all-one vector.

the following subsection is subjected to apply the MoG distribution for remodeling the PDF of Z.

B. MIXTURE OF GAUSSIAN (MoG) DISTRIBUTION

For the purpose of differentiating the Fox-based result, $f_{\hat{\mathsf{Z}}}(z)$ and $F_{\hat{\mathsf{Z}}}(z)$ are utilized herein to denote the MoG-based PDF and CDF, given by

$$f_{\hat{\mathsf{Z}}}(z) = \sum_{l=1}^{C} \frac{w_l}{\sqrt{2\pi}\,\eta_l} \exp\left(-\frac{(z-\varsigma_l)^2}{2\eta_l^2}\right), \tag{4a}$$

$$F_{\hat{\mathsf{Z}}}(z) = \sum_{l=1}^{C} \frac{w_l}{2}\left(1 + \mathrm{erf}\left(\frac{z-\varsigma_l}{\sqrt{2}\eta_l}\right)\right), \tag{4b}$$

where C represents the number of Gaussian components.[3] $w_l > 0$, ς_l and η_l are respectively the lth weight, mean, and variance with the constraint of $\sum_{l=1}^{C} w_l = 1$.

As shown in Fig. 1, we have plotted the PDF of Z for selected value of M, where α and μ is chosen as an illustrative example based on the experimental and analytical results obtained in [34]–[39], the corresponding estimated parameters, i.e., C, w_l, ς_l, η_l when $M = 3$, are provided in Table 1. Interestingly, one can observe that there exists a highly close agreement between the simulated and approximated PDFs. Besides, the MoG distribution not only can model both the composite and non-composite fading channels, herein we prove that the MoG distribution is also beneficial to offer a simple but effective approach to model the sum of M versions of cascaded α-μ distributed RVs.

TABLE 1. MoG parameters for Z over cascaded α-μ fading channels when $\alpha = 4.5$, $\mu = 3.5$, $M = 3$, $N = 2$, and $C = 2$.

l	w_l	ς_l	η_l
1	0.224375	3.025526	0.299281
2	0.775625	2.770252	0.289974

C. APPROXIMATION ACCURACY

In order to evaluate the accuracy of the MoG distribution, the KS goodness of fit test is accordingly conducted [23], [53]. The KS test statistic D is to maximize the difference between the simulated and approximated CDFs, i.e.,

$$D \triangleq \max |F_{\mathsf{Z}}(z) - F_{\hat{\mathsf{Z}}}(z)||, \tag{5}$$

where $F_{\mathsf{Z}}(z)$ is the empirical CDF of RV Z, and $F_{\hat{\mathsf{Z}}}(z)$ is the approximated CDF given in (4b). Let the hypothesis H_0 denotes that Z follows the MoG distribution. Such an hypothesis is accepted only when D is smaller than the critical value D_{max}, i.e., $D < D_{max}$, which is given by

$$D_{max} \approx \sqrt{-(1/2v)\ln(\tau/2)},$$

[3]The number of components C is selected automatically using the Bayesian information criterion (BIC) method given in [51, Section III-C] whereas the corresponding parameters for the MoG distribution are evaluated using the EM algorithm.

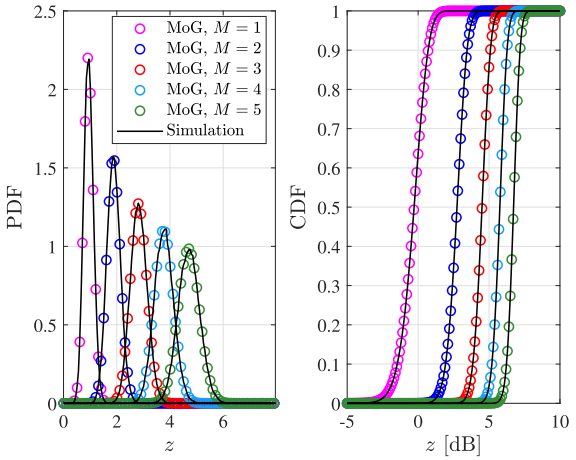

FIGURE 1. The PDF and CDF of Z over cascaded α-μ (i.e., $\alpha = 4.5$, $\mu = 3$) fading channels for selected values of M, where $N = 2$.

where τ is the significance level, and v is the number of random samples of Z.

Obviously, Fig. 1 presents that the MoG-based CDF of Z approximated the Monte-Carlo simulation results with good accuracy. The KS test statistic D obtained from Fig. 1 when $M = 1, \cdots, 5$ are respectively given as 2.2×10^{-3}, 2.3×10^{-3}, 1.6×10^{-3}, 2.8×10^{-3}, and 1.7×10^{-3}. Herein, in our KS goodness of fit test, let $\alpha = 5\%$, and $v = 10^5$. Thus, we have $D_{max} = 0.0043 = 4.3 \times 10^{-3}$. The hypothesis H_0 is surely accepted for the cases $M = 1, \cdots, 5$ due to $D < D_{max}$.

III. SYSTEM MODEL FOR RIS-AIDED COMMUNICATIONS

As discussed in Section I, the application of cascaded fading channels is widely used in many communication scenarios, e.g., M2M communications, multihop AF relaying communication, MIMO keyhole/pinhole systems, and also the newly proposed RIS-enabled communication systems. To this end, in the following subsection, we have introduced the RIS-aided wireless communication systems as an illustrative application of the preliminary results.

A. SYSTEM MODEL

Suppose a source node (**S**) intends to transmit messages to a destination (**D**) with the assistance of an RIS, as shown in Fig. 2 [54], which is composed of M passive and low-cost reflectors. It is assumed that both **S** and **D** are equipped with a single antenna. The instantaneous received signal at **D** is

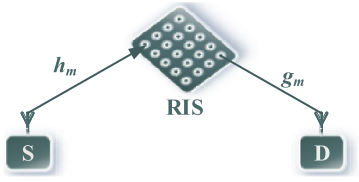

FIGURE 2. A wireless communication system configuration with one source (S) and one destination (D) assisted with an RIS.

given by

$$y_D = \sqrt{E_s}\left|\sum_{m=1}^{M} h_m u_m g_m\right| s + \mathfrak{n}, \tag{6}$$

where E_s is the transmit power, $h_m = \mathfrak{h}_m \exp(-w\phi_m)$ and $g_m = \mathfrak{g}_m \exp(-w\psi_m)$ are independent and identically distributed (i.i.d.) α-μ RVs,[4] which correspond to the channel coefficients from **S** to the m-th reflector element and the m-th reflector element to **D**, respectively. $\mathfrak{h}_m$, $\mathfrak{g}_m$, ϕ_m, and ψ_m denote the amplitudes and phases of the corresponding fading channel gains. $u_m = \mathfrak{w}_m(\theta_m)\exp(w\theta_m)$ is the reflection coefficient produced by the m-th element of the RIS, herein $\mathfrak{w}_m(\theta_m) = 1$ for the ideal phase shifts, $m = 1, \cdots, M$. s is the transmitted signal with unit energy. $\mathfrak{n}$ is the additive white Gaussian noise (AWGN) with zero mean and N_0 variance.

The instantaneous received effective SNR at **D**, γ_D, is expressed as

$$\gamma_D = \frac{E_s}{N_0}\left|\sum_{m=1}^{M} \mathfrak{h}_m \mathfrak{g}_m \exp\left(w(\theta_m - \phi_m - \psi_m)\right)\right|^2. \tag{7}$$

Considering the best case, namely, to maximize γ_D, the channel phase is similarly eliminated with [54], i.e, let $\theta_m = \phi_m + \psi_m$ for all $m = 1, \cdots, M$. As such, γ_D is then represented as

$$\gamma_D = \frac{E_s}{N_0}\left|\sum_{m=1}^{M} \mathfrak{h}_m \mathfrak{g}_m\right|^2 = \bar{\gamma}\left|\sum_{n=1}^{M} \mathbb{W}_m\right|^2, \tag{8}$$

where $\bar{\gamma} = \frac{E_s}{N_0}$ and $\mathbb{W}_m = \mathfrak{h}_m \mathfrak{g}_m$. Since $\mathfrak{h}_m$ and $\mathfrak{g}_m$ are i.i.d. α-μ distributed RVs, using the result obtained in [24, Theorem 1], one can observe that $\mathbb{W}_m$ follows the cascaded α-μ distribution. In other words, the link between **S** and **D** via a reflector surface can be modeled by the cascaded fading distribution.

Again let $\mathcal{Y} = \sum_{m=1}^{M} \mathbb{W}_m$, apparently $\mathcal{Y}$ is the sum of M versions of cascaded α-μ distributed RVs. Performing the interchange of RV $\mathcal{Y} = \sqrt{\frac{\gamma_D}{\bar{\gamma}}}$, and applying the results given in (3) and (4a), the exact and MOG-approximated PDF of $\gamma_D = \bar{\gamma}\mathcal{Y}^2$ are thereafter given by

$$f_D(\gamma) = \frac{1}{2\sqrt{\bar{\gamma}\gamma}} f_Z\left(\sqrt{\frac{\gamma}{\bar{\gamma}}}\right), \tag{9a}$$

$$f_{\hat{D}}(\gamma) = \sum_{l=1}^{C} \frac{w_l}{\sqrt{8\pi\bar{\gamma}\eta_l\sqrt{\gamma}}} \exp\left(-\frac{(\sqrt{\gamma/\bar{\gamma}} - \varsigma_l)^2}{2\eta_l^2}\right). \tag{9b}$$

IV. EFFECTIVE RATE ANALYSIS

A. DEFINITION OF EFFECTIVE RATE

Assuming the block fading channel, the normalized effective rate is given as [14]

$$\mathcal{R} = -\frac{1}{A}\log_2\underbrace{\left[\mathbb{E}\left((1+\gamma_D)^{-A}\right)\right]}_{\mathcal{U}} \text{ bit/s/Hz}, \tag{10}$$

[4]When the RIS is far away from **S** and **D**, it is assumed that $\mathfrak{h}_m$ and $\mathfrak{g}_m$ may be regarded as independent of the RIS element [55].

where $A = \frac{\theta TB}{\ln(2)}$, where $\theta > 0$, T, and B represent the delay exponent, the block length, and the system bandwidth, respectively. The QoS exponent θ is defined from the delay outage probability, which is mathematically formulated as

$$\theta = -\lim_{Q_{max}\to\infty} \frac{\ln\left(Pr(Q \geq Q_{max})\right)}{Q_{max}},$$

where $Pr(a \geq b)$ stands for the probability of a being larger than or equal to b. Herein, Q denotes the queue length at the transmitter buffer side, and Q_{max} is the predetermined threshold of the queue length. Practically speaking, $\theta \to 0$ implies the delay-tolerant communication, while $\theta \to \infty$ implies the delay-limited communication [56], e.g., voice calls.

B. EXACT EFFECTIVE RATE ANALYSIS

Theorem 1: The effective rate of the RIS-assisted communications over α-μ fading channel is given by

$$\mathcal{R}_M = -\frac{1}{A}\log_2\left[\frac{\eta_M}{\Gamma(A)}\Delta\right], \quad \textit{where}$$

$$\Delta = H\left(\begin{matrix}\binom{1,1}{1,2}\\ \binom{N_j,1}{1,N_j}_{j=1:M}\end{matrix}\middle|\begin{matrix}(1;\frac{1}{2}1_M)\\ (A;1\frac{1}{2}1_M),(1;1_M)\\ \left[(1,1)\right]_{j=1:M}\\ \mathscr{B}\end{matrix}\middle|\left(\frac{\mathcal{C}_{N,j}}{\sqrt{(\gamma)}}\right)_{j=1:M}\right). \tag{11}$$

Proof: See Appendix VI. ∎

Remark 1: When $M = 1$, the effective rate of the RIS-assisted communications over α-μ fading channel is given by

$$\mathcal{R}_S = -\frac{1}{A}\log_2 \times\left(\frac{\mathcal{K}_N}{2\sqrt{\bar{\gamma}}\Gamma(A)} H_{1,N+1}^{N+1,1}\left[\frac{\mathcal{C}_N}{\sqrt{\bar{\gamma}}}\middle|\begin{matrix}(\frac{1}{2},\frac{1}{2})\\ \mathcal{B},(A-\frac{1}{2},\frac{1}{2})\end{matrix}\right]\right). \tag{12}$$

Proof: When $M = 1$, we have $\gamma_D = \bar{\gamma}|\mathbb{W}_1|^2 = \bar{\gamma}\mathcal{Y}^2$. Next, applying the result given in (2), the PDF of γ_D is given by

$$f_D(\gamma) = \frac{\mathcal{K}_N}{2\sqrt{\bar{\gamma}\gamma}} H_{0,N}^{N,0}\left[\mathcal{C}_N\sqrt{\frac{\gamma}{\bar{\gamma}}}\middle|\begin{matrix}-\\ \mathcal{B}\end{matrix}\right]. \tag{13}$$

Re-expressing

$$\frac{1}{(1+x)^A} = \frac{1}{\Gamma(A)} H_{1,1}^{1,1}\left[x\middle|\begin{matrix}(1-A,1)\\ (0,1)\end{matrix}\right], \tag{14}$$

in terms of Meijer's G-function [57, Chpt. 8.4], then plugging (14) and (13) into $\mathcal{U}$, yields

$$\mathcal{U} = \frac{\mathcal{K}_N}{2\Gamma(A)\sqrt{\bar{\gamma}}}\int_0^\infty \frac{1}{\sqrt{\gamma}} H_{1,1}^{1,1}\left[\gamma\middle|\begin{matrix}(1-A,1)\\ (0,1)\end{matrix}\right] \times H_{0,N}^{N,0}\left[\mathcal{C}_N\sqrt{\frac{\gamma}{\bar{\gamma}}}\middle|\begin{matrix}-\\ \mathcal{B}\end{matrix}\right] d\gamma, \tag{15}$$

subsequently applying the Mellin transform of two Fox's H-function [57, Eqs.(2.25.1.1) and (8.3.2.21)], the proof is accomplished. ∎

As stated earlier, the cascaded α-μ distribution encompasses the cascaded Rayleigh and Nakagami-m distributions, utilizing the property of Fox's H-function [57, Eq.(8.3.2.21)], the effective rate of the RIS-assisted communications over Nakagami-m ($\mu = m$) and Rayleigh ($\mu = m = 1$) fading channel when $M = 1$ are expressed as follows, in terms of the Meijer's G-function, i.e., $G_{p,q}^{m,n}(\cdot)$,[5]

$$\mathcal{R}_S = -\frac{1}{A}\log_2\left(\frac{\mathcal{K}_N}{\mathcal{C}_N\Gamma(A)}\Delta\right), \quad \text{where}$$
$$\Delta = \begin{cases} G_{1,N+1}^{N+1,1}\left[\dfrac{\mathcal{C}_N^2}{\bar{\gamma}}\middle|\begin{matrix}1\\ m1_N, A\end{matrix}\right], & \text{Nakagami-}m, \\ G_{1,N+1}^{N+1,1}\left[\dfrac{\mathcal{C}_N^2}{\bar{\gamma}}\middle|\begin{matrix}1\\ 1_N, A\end{matrix}\right], & \text{Rayleigh.}\end{cases} \tag{16}$$

Proof: When $\alpha = 2$, then deploying the elementary property of Fox's H-function [58, Eqs. (2.1.5), (2.1.4), and (2.9.1)], the proof is obtained. ■

C. ASYMPTOTIC EFFECTIVE RATE ANALYSIS

Remark 2: The asymptotic behavior of effective rate over α-μ fading channel at high SNR regime when $M = 1$ is given by

$$\mathcal{R}_S^{\infty} \approx -\frac{1}{A}\log_2\left(\frac{\kappa_N}{2\sqrt{\bar{\gamma}}\Gamma(A)}\Delta^{\infty}\right), \quad \textit{where}$$
$$\Delta^{\infty} = \begin{cases} 2\Gamma(A)\displaystyle\prod_{i=1}^{N}\Gamma\left(\mu_i - \frac{2A}{\alpha_i}\right)\left(\frac{\mathcal{C}_N}{\sqrt{\bar{\gamma}}}\right)^{2A-1}, & 2A < \tau, \\ \displaystyle\prod_{i=1, i\neq c}^{N}\frac{\alpha_c\Gamma\left(A-\frac{\tau}{2}\right)\Gamma\left(\frac{\tau}{2}\right)\Gamma\left(\mu_i-\frac{\tau}{\alpha_i}\right)}{\left(\frac{\mathcal{C}_N}{\sqrt{\bar{\gamma}}}\right)^{1-\tau}}, & 2A > \tau. \end{cases} \tag{17}$$

Proof: Assuming all the residues of the Fox's H-function are simple, when $\bar{\gamma}$ goes to ∞, we have $\frac{\mathcal{C}_N}{\sqrt{\bar{\gamma}}} \to 0$, the asymptotic behavior of (12) is evaluated at $\xi = 1 - \min(\tau, 2A)$ where

$$\tau = \min_{i=1,\cdots,N}\alpha_i\mu_i, \quad c = \arg\min_{i=1,\cdots,N}\alpha_i\mu_i, \tag{18}$$

subsequently making expansion of (12) at $s = \xi$ [59], and using the residue theorem [60] under the constraint $A < \frac{\tau}{2}$, we have

$$\Delta^{\infty} \approx \text{Res}\left[\prod_{i=1}^{N}\Gamma\left(\mu_i - \frac{1}{\alpha_i} + \frac{s}{\alpha_i}\right)\Gamma\left(A - \frac{1}{2} + \frac{s}{2}\right) \times \Gamma\left(\frac{1}{2} - \frac{s}{2}\right)\left(\frac{\mathcal{C}_N}{\sqrt{\bar{\gamma}}}\right)^{-s}, 1 - 2A\right]$$
$$= \lim_{s\to 1-2A}\prod_{i=1}^{N}2\Gamma\left(\mu_i - \frac{1}{\alpha_i} + \frac{s}{\alpha_i}\right)\Gamma\left(\frac{1}{2} - \frac{s}{2}\right)\left(\frac{\mathcal{C}_N}{\sqrt{\bar{\gamma}}}\right)^{-s}$$
$$= 2\Gamma(A)\prod_{i=1}^{N}\Gamma\left(\mu_i - \frac{2A}{\alpha_i}\right)\left(\frac{\mathcal{C}_N}{\sqrt{\bar{\gamma}}}\right)^{2A-1}. \tag{19}$$

The case $2A < \tau$ is similarly accomplished. ■

The exact effective rate is expressed in terms of the multivariate Fox's H-function, the asymptotic behavior of effective rate is further provided to gain more insights at the high SNR regime.

Remark 3: The asymptotic behavior of effective rate at high SNR regime is given by under the condition that $2A > \sum_{j=1}^{M}\xi_j$,

$$\mathcal{R}_M^{\infty} \approx -\frac{1}{A}\log_2\left[\frac{\eta_M}{2\Gamma(A)}\Gamma\left(A - \sum_{j=1}^{M}\frac{\xi_j}{2}\right)\frac{\Gamma\left(\sum_{j=1}^{M}\frac{\xi_j}{2}\right)}{\Gamma\left(\sum_{j=1}^{M}\xi_j\right)} \times\prod_{j=1}^{M}\lim_{s\to\xi_j}(s_j - \xi_j)\prod_{i=1, i\neq c}^{N}\Gamma\left(\mu_i - \frac{\xi_j}{\alpha_i}\right)\Gamma(\xi_j)\left(\frac{\mathcal{C}_{N,j}}{\sqrt{\bar{\gamma}}}\right)^{\xi_j}\right],$$

where

$$\xi_j = \min_{i=1,\cdots,N}\alpha_{j,i}\mu_{j,i}, \quad c = \arg\min_{i=1,\cdots,N}\alpha_{j,i}\mu_{j,i}. \tag{20}$$

Especially when $N = 1$, (11) is then expanded at $\xi_j = \alpha_j\mu_j$ with constraint $2A - \sum_{j=1}^{M}\xi_j > 0$.

$$\mathcal{R}_M^{\infty} \approx -\frac{1}{A}\log_2\left[\frac{\eta_M}{2\Gamma(A)}\frac{\Gamma\left(A - \sum_{j=1}^{M}\frac{\xi_j}{2}\right)\left(\sum_{j=1}^{M}\frac{\xi_j}{2}\right)}{\Gamma\left(\sum_{j=1}^{M}\xi_j\right)} \times\prod_{j=1}^{M}\alpha_j\Gamma\left(\xi_j\right)\left(\frac{\mathcal{C}_{N,j}}{\sqrt{\bar{\gamma}}}\right)^{\xi_j}\right]. \tag{21}$$

Proof: See Appendix VI. ■

Remark 4: Observing from (17) and (20), the high SNR slope of effective rate is defined as

$$S^{\infty} = \frac{\mathcal{R}^{\infty}}{\log_2\bar{\gamma}}, \tag{22}$$

subsequently, substituting $\mathcal{R}_S^{\infty}$ and $\mathcal{R}_M^{\infty}$ into (22), we have

$$S_S^{\infty} = \begin{cases} 1, & 2A < \tau, \\ \dfrac{\tau}{A}, & 2A > \tau. \end{cases} \tag{23a}$$

$$S_M^{\infty} = \frac{1}{A}\sum_{j=1}^{M}\frac{\xi_j}{2}, \quad 2A > \sum_{j=1}^{M}\xi_j, \tag{23b}$$

where τ and ξ_j are given in (18) and (20), respectively.

As discussed in this Section, the exact and asymptotic behaviors of the effective rate for the RIS-assisted system setup are characterized. It is noted that the exact effective rate is derived with closed-form expression, given in terms of the multivariate Fox's H-function. In the following subsection, the highly tight effective rate with the assistance of the MoG distribution is derived.

[5]Note that the univariate Meijer's G-function is available, i.e., MATLAB meijerG(a, b, c, d, x), Maple MeijerG($[a_s, b_s], [c_s, d_s], z$), and Mathematica MeijerG[$\{a_i\}_{i=1:n}, \{a_i\}_{i=n+1:p}, \{b_i\}_{i=1:m}, \{b_i\}_{i=m+1:q}, z$].

D. AN ALTERNATIVE APPROXIMATION METHOD

Remark 5: Motivated by (9b), one can observe that γ_D can be modeled in terms of the C normally distributed random variable, i.e., $\gamma_D = \sum_{l=1}^{C} \gamma_l$, and $\gamma_l \backsim \mathcal{N}(\varsigma_l, \eta_l)$, consequently, the effective rate of our proposed system configuration can be highly approximated as follows

$$\mathcal{R}^{MoG} \approx -\frac{1}{A}\log_2\left[\sum_{l=1}^{C} w_l \left(\frac{2}{3(1+\bar{\gamma}\varsigma_l^2)^A} + \frac{1}{6(1+\bar{\gamma}(\varsigma_l+\sqrt{3}\eta_l)^2)^A} + \frac{1}{6(1+\bar{\gamma}(\varsigma_l-\sqrt{3}\eta_l)^2)^A}\right)\right]. \tag{24}$$

Proof: Performing a revisit to $\mathcal{U}$ given in (10), then substituting (9b) into $\mathcal{U}$, yields

$$\mathcal{U} = \sum_{l=1}^{C} \frac{w_l}{\sqrt{8\pi\bar{\gamma}\eta_l}} \int_0^\infty \frac{\gamma^{-\frac{1}{2}}}{(1+\gamma)^A} \exp\left(-\frac{(\sqrt{\gamma/\bar{\gamma}}-\varsigma_l)^2}{2\eta_l^2}\right) d\gamma \overset{(c)}{=} \sum_{l=1}^{C} \frac{w_l}{\sqrt{2\pi}\eta_l} \int_0^\infty \frac{1}{(1+\bar{\gamma}y^2)^A} \exp\left(-\frac{(y-\varsigma_l)^2}{2\eta_l^2}\right) dy, \tag{25}$$

where step (c) is developed by interchanging of variables $y = \sqrt{\frac{\gamma}{\bar{\gamma}}}$, then applying the result given in [61, Eq. (4)], i.e., $\mathcal{F}(y) = \frac{1}{(1+\bar{\gamma}y^2)}$ is a real function of y, herein y follows the normal distribution with mean ς_l and variance η_l, the expectation of $\mathcal{F}(y)$ can be highly approximated at three points, namely, ς_l, $\varsigma_l + \sqrt{3}\eta_l$, and $\varsigma_l - \sqrt{3}\eta_l$ [62],

$$\mathcal{E}[\mathcal{F}(y)] \approx \mathcal{F}(\varsigma_l) + \mathcal{F}(\varsigma_l + \sqrt{3}\eta_l) + \mathcal{F}(\varsigma_l - \sqrt{3}\eta_l). \tag{26}$$

Finally, substituting (26) into (10), the proof is accomplished. ■

V. NUMERICAL RESULTS AND DISCUSSION

For the simplicity of notifications, assuming that all M version of cascaded α-μ distributed RVs have the same fading parameters, i.e., $\alpha_1 = \cdots = \alpha_N = \alpha$, and $\mu_1 = \cdots = \mu_N = \mu$ in the simulation. The α-μ distributed RVs are implemented using the WAFO toolbox [63]. It is noteworthy that in this paper when $M = 1$, N is an integer, which corresponds to the multi-hop AF non-regenerative relaying system [22] or MIMO keyhole systems [21]; when $N = 1$, M is an integer, which might probably be single-hop multiple-input single-output (MISO) systems [10]; and when $N = 2$, and M is an integer, it is the RIS-aided system under consideration.

Currently, no existing mathematical packages are available at MATLAB, Python, or Mathematica to compute the multivariate Fox's H-function, but it is still numerically programmable and computable, see existing examples using Python code [50] and MATLAB code [64]. The multivariate Fox's H-function is implemented herein by using the method given in [50].

A. NUMERICAL RESULTS

As shown in Fig. 3 (a) and (b), the effective rate of the RIS-assisted communications over α-μ fading channels given in (11) and **Remark**. 5 is presented for selected values of M and N. One can conclude that 1) the effective rate certainly increases as M increases; 2) $\mathcal{R}$ decreases as N increases; and 3) in addition, the effective rate expression derived in **Remark**. 5 provides a highly tight approximation to the exact result. This fact can be further confirmed in the following subsection. Besides, the MoG-based effective rate expression becomes gradually tight as N decreases and M increases, respectively.

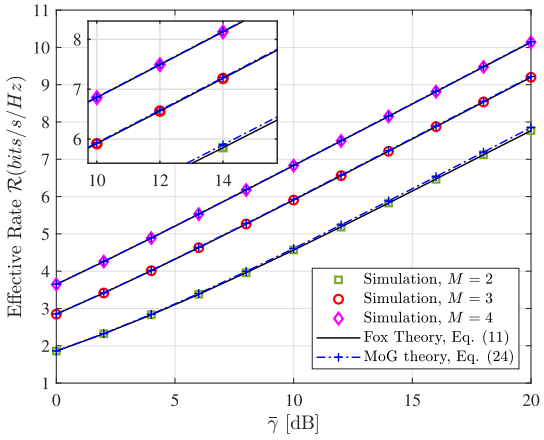

(a) $N = 2$

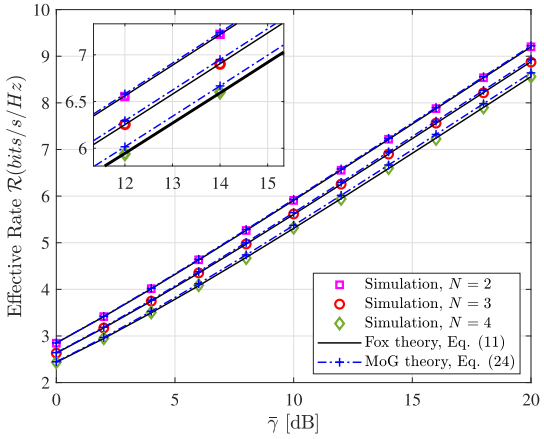

(b) $M = 3$

FIGURE 3. Effective rate over α-μ fading channels against $\bar{\gamma}$ for selected values of M and N, where $A = 4$, and $\alpha = \mu = 3$.

The asymptotic behavior of effective rate at high SNR regime is depicted in Fig. 4, the analytical behavior of $\mathcal{R}$ given in (20) becomes gradually tight when $\bar{\gamma}$ increases. One can observe that when $N = 1$, $\alpha = 2$, $\mu = 1$, and $A = 4$, the values of effective rate at 40 dB and 30 dB when $M = 1, 2, 3$ are 3.718, 7.686, 11.59 and 2.888, 6.011, 9.081, respectively. As a result, the slopes of the asymptotic effective rate $\mathcal{R}_M^\infty$ when $M = 1, 2, 3$ are correspondingly given by

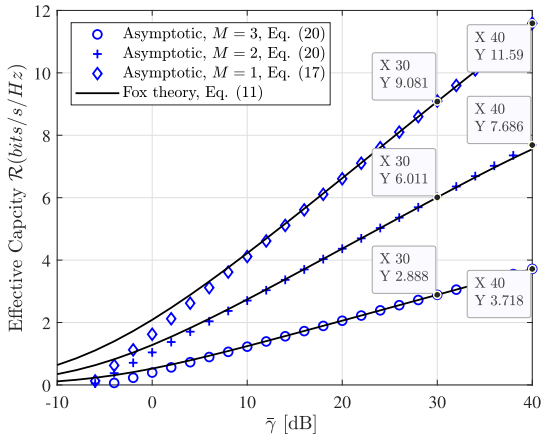

FIGURE 4. Effective rate over α-μ (i.e., $\alpha = 2$, $\mu = 1$) fading channels against $\bar{\gamma}$, where $N = 1$ and $A = 4$.

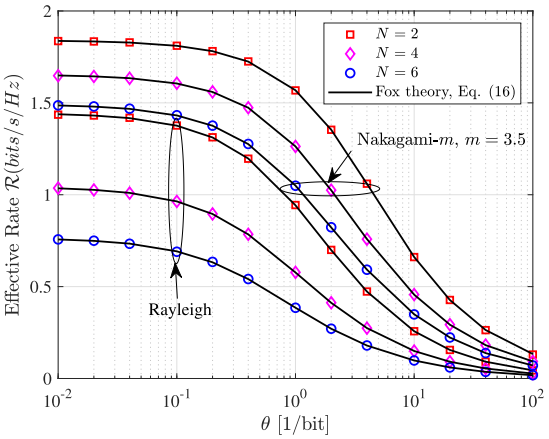

FIGURE 5. Effective rate over Rayleigh ($\mu = 1$) and Nakagami-m ($\mu = m = 3.5$) fading channels against θ for selected values of N, where $A = \frac{\theta TB}{\ln(2)}$, $TB = 1$, and $M = 1$.

$(3.718 - 2.888) \times \log_{10}(2) = 0.2499 \approx 0.25 = \frac{\tau}{2A} = \frac{\alpha\mu}{2A}$, $(7.686 - 6.011) \times \log_{10}(2) = 0.5042 \approx 0.5 = \frac{\tau}{2A} = \frac{\alpha\mu}{A}$, and $(11.59 - 9.081) \times \log_{10}(2) = 0.7553 \approx 0.75 = \frac{3\tau}{2A} = \frac{3\alpha\mu}{2A}$. Overall, the asymptotic slope of effective rate given in (23b) is verified, and the asymptotic analysis at high SNR regime is proved to be efficient with reducing complexity compared to the exact effective rate expression. One can obtain that the high SNR slope is linearly associated with α and μ. More specifically, large α and μ lead to a steep high SNR slope curve. In other words, large α and μ contributes to higher effective rate performance. Such a conclusion is also verified in Figs. 5 and 8, which is because the increase of α and μ physically accounts for the less severe fading environment.

In Fig. 5, the effective rate over Rayleigh and Nakagami-m ($m = 3.5$) fading channels, given in (16), are compared versus the delay QoS exponent θ. We observe that the gain in effective rate degrades as the QoS limitation becomes stricter. As discussed in [22], the cascaded Rayleigh distribution was found feasible to model the M2M communication scenario, an increase of N herein means the increase of hops, resultantly leading to a worse effective rate performance. The impact of N and fading parameter μ are also presented. One can observe that the effective rate is improved with the increase of fading parameter μ, i.e., multipath fading parameter.

Fig. 6 presents the asymptotic effective rate at high SNR regime, together with the exact and simulated results. One can observe that the analytical asymptotic effective rate, as expected, gradually behaves accurately as $\bar{\gamma}$ increases. Besides, inspired by [18], we also verified the asymptotic effective rate slope at high SNR regime, theoretically given in (23a), for $N = 2$, the $\mathcal{R}_S^\infty$ is 15.02 and 11.7 at 50 dB and 40 dB, respectively. The high SNR slope is then computed as $(15.02 - 11.7) \times \log_{10}(2) = 0.9994 \approx 1$. Consequently, as $\bar{\gamma}$ increases, then S_S^∞ will surely converge to 1.

In Fig. 7, we investigate the effective rate of the proposed RIS-assisted system, where the number of reflecting elements of the RIS ranges from 100, 150, 200, 300, 400,

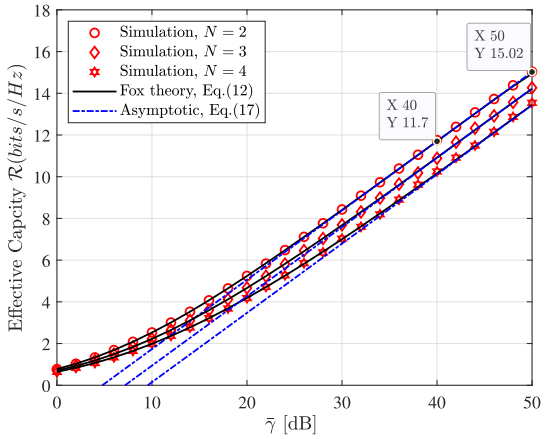

FIGURE 6. Effective rate over α-μ fading channels against $\bar{\gamma}$, where $M = 1$, $A = 3$, $\alpha = 2$, and $\mu = 5$.

and 500. A perfect match between the Monte-Carlo simulation and the MoG-based analytical results is validated. It is noteworthy that the exact effective rate expression becomes difficult and time-consuming to implement the multivariate Mellin-Barnes integrals as M becomes larger, e.g., 200. Conclusively, the MoG-based solution alternatively showcases its importance and high priority when doing performance calculation compared to the multivariate Fox's H-function based solution.

Fig. 8 plots the effective rate of the RIS-aided system against θ over Weibull (α is the fading parameter, and $\mu = 1$) fading channels with consideration of the impacts from the fading parameter α. One can observe that (i) the increase of α is beneficial for $\mathcal{R}$. More importantly, the gain in effective capacity benefiting from the increase of α becomes obvious as the QoS limitation θ tends to high, which is quite different from Fig. 5; (ii) as expected, the effective rate demonstrates an improvement as A decreases, in other words, a smaller delay constraint results in a higher effective rate performance; and (iii) as shown in Fig. 5, the multipath

TABLE 2. Analytical error against $\bar{\gamma}$(*dB*) when $A = 4, M = 4, N = 2, \alpha = \mu = 3$.

$\mathcal{R}$ \ $\bar{\gamma}$	0	4	8	12	16	20
error_{Fox}	$-1.92 * 10^{-3}\%$	$3.05 * 10^{-2}\%$	$2.17 * 10^{-2}\%$	$5.34 * 10^{-4}\%$	$1.76 * 10^{-2}\%$	$-5.19 * 10^{-3}\%$
error_{MoG}	-0.13%	-0.11%	-0.11%	-0.12%	$-8.74 * 10^{-2}\%$	$-9.86 * 10^{-2}\%$

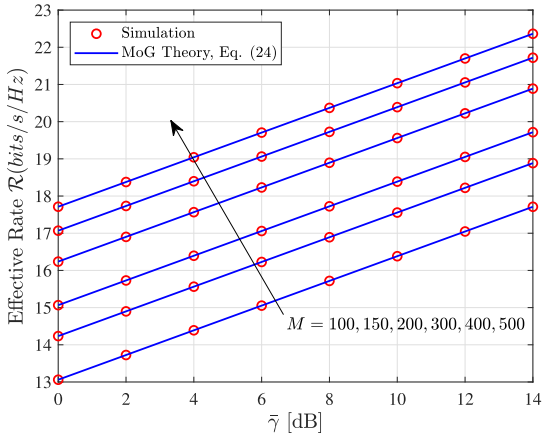

FIGURE 7. Effective rate over α-μ fading channels against $\bar{\gamma}$, where $A = 4$, $N = 2$, and $\alpha = \mu = 3$.

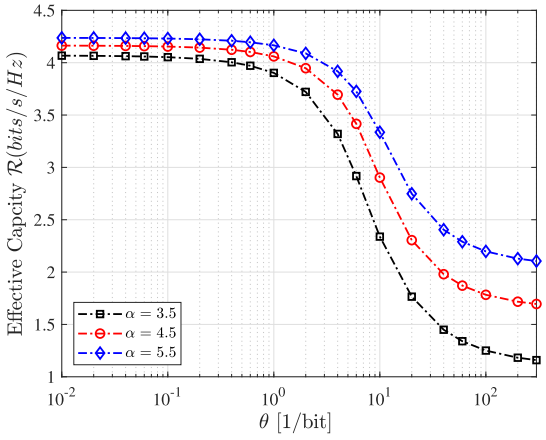

FIGURE 8. Effective rate over Weibull (α is the fading parameter, $\mu = 1$) fading channels against θ, where $A = \frac{\theta TB}{\ln(2)}$, $N = 2$, $M = 5$, and $\bar{\gamma} = 0$ dB.

effect has a negative impact on the effective rate performance, i.e., lower values of α and μ, which indicate the serious nonlinearity and sparse clustering of propagation medium, lead to the poor effective rate performance.

B. ACCURACY ANALYSIS

For the purposes of illustrating the tightness of our analytical results, a useful measure, namely analytical error, is used as the accuracy indicator [52], [61],

$$\text{analytical error} = 1 - \frac{\text{analytical results}}{\text{simulation results}} \times 100\%. \quad (27)$$

For the brevity of notations, let error_{Fox} denote the analytical error between the simulated results and the Fox's H-function based results, similarly, error_{MoG} represents the analytical error between the simulated results and the MoG-based results.

Based on Fig. 3. (a), as shown in Table. 2, we have two interesting observations: (i) both error_{Fox} and error_{MoG} ranges from -1% to 1%, such a fact can be interpreted that both results are highly accurate; and (ii) compared with error_{Fox}, error_{MoG} is always negative. Such a fact indicates that the MoG-based expression acts as a highly tight upper bound for the exact effective rate.

VI. CONCLUSION

In this paper, we have characterized the sum of cascaded α-μ RVs, and studied its application in the RIS-assisted communications from the effective rate perspective. The exact, asymptotic, and approximated behaviors of the effective rate performance for the RIS-aided communications are explored and further derived with closed-form expressions. The asymptotic effective rate slope at high SNR regime was also provided. The accuracy of our analytical results were supported by the simulated results, and tightly approached by its asymptotic behavior at high SNR regime.

Interesting and useful insights can be thereafter obtained that (i) the obtained analytical results are not only applicable for the RIS-aided systems, when $M = 1$ or $N = 1$, it corresponds to the multi-hop AF non-regenerative relaying system [22]/MIMO keyhole systems [21] or the single-hop MISO systems [10]; (ii) the effective rate can take advantage of the increase of M and the decrease of the number of statistically independent scatters N; and (iii) fading parameters, α and μ, i.e., nonlinearity and clustering of the wireless propagation medium, are advantageous to enhance the effective rate performance. In addition, compared with the multivariate Fox's H-function based effective rate expression, the MoG-based solution is highly accurate and serves as a tight and simple upper bound for the exact effective rate solution with reducing complexity. Overall, this paper mainly considered the ideal phase-shifting, the correlation of signals in RIS-aided systems is a worthy subject and left for future investigation.

APPENDIX A
PROOF FOR THEOREM 1

Revisiting the multivariate Fox's H-function in (9a) in terms of its definition from (3), and then Plugging the result and (14) into $\mathcal{U}$, we have $\mathcal{U}$ given in (28), shown at the

bottom of the page. It is noted that step (d) in (28) is developed by interchanging the order of two integrals, subsequently, $\mathcal{U}_1$ is further evaluated with the help of the definition of Mellin transform for Fox's H-function [57, Eq.(2.25.2.1)],

$$\mathcal{U}_1 = \Gamma\left(\sum_{j=1}^{M}\frac{s_j}{2}\right)\Gamma\left(A-\sum_{j=1}^{M}\frac{s_j}{2}\right). \tag{29}$$

After some algebraic manipulations and deploying the definition of multivariate Fox's H-function, the effective rate of the RIS-assisted system setup over α-μ fading channel is obtained.

APPENDIX B
PROOF FOR REMARK 3

Since the exact effective rate expression is given in terms of the multivariate Fox's H-function, then re-expressing the multivariate Fox's H-function in the manner of the multiple Mellin-Barnes type integral according to its definition. When $\bar{\gamma}\to\infty$, we have

$$\frac{\mathcal{C}_{N,j}}{\sqrt{\bar{\gamma}}} = \frac{1}{\sqrt{\bar{\gamma}}}\prod_{i=1}^{N}\frac{\mu_{i,j}^{\frac{1}{\alpha_{i,j}}}\Gamma\left(\mu_{i,j}+\frac{1}{\alpha_{i,j}}\right)}{\Gamma(\mu_{i,j})}\to 0.$$

Applying the result given in [59], each single Mellin-Barnes integral is then further simplified and expanded at the single residue ξ_j of the corresponding integrands at the pole closest to the contour [47], namely, the minimum pole on the right of the contour for small Fox's H arguments, and subsequently applying the residue theorem, we can arrive at (20).

To be specific, we herein take the case $M=3$ and $N=1$ as an example to illustrate the steps for arriving at the asymptotic effective rate behavior. As such, the effective rate is re-expressed as follows in terms of the definition of multivariate Fox's H-function,

$$\mathcal{R} = -\frac{1}{A}\log_2\left[\frac{\eta_M}{2\Gamma(A)}\Delta\right], \quad \text{where}$$
$$\Delta = \frac{1}{(2\pi w)^3}\int_{\mathcal{L}_1}\int_{\mathcal{L}_2}\int_{\mathcal{L}_3}\mathsf{K}(s_1,s_2,s_3)ds_1ds_2\,ds_3,$$

and

$$\begin{cases}\mathsf{K}(s_1,s_2,s_3) = \Phi(s_1,s_2,s_3)\prod_{j=1}^{3}\phi(s_j)\left(\frac{\mathcal{C}_{1,j}}{\sqrt{\bar{\gamma}}}\right)^{s_j}\\ \Phi(s_1,s_2,s_3) = \frac{\Gamma\left(A-\frac{s_1+s_2+s_3}{2}\right)\Gamma\left(\frac{s_1+s_2+s_3}{2}\right)}{\Gamma(s_1+s_2+s_3)}\\ \phi(s_j) = \Gamma\left(\mu_j-\frac{1}{\alpha_j}s_j\right)\Gamma(s_j),\quad j=1,2,3.\end{cases} \tag{30}$$

When $\bar{\gamma}$ goes to ∞, we have $\frac{\mathcal{C}_{1,j}}{\sqrt{\bar{\gamma}}}\to 0$. According to [58, Theorem 1.7], the Mellin-Barnes integral over $\mathcal{L}_1$ is approximated by evaluating the residue at the closest pole located to the right-hand side, i.e., $\xi_1=\alpha_1\mu_1$. As such, the contour $\mathcal{L}_1$ is clockwise and -1 is needed to be multiplied, [47]

$$\begin{aligned}\Delta &= \frac{1}{(2\pi w)^3}\int_{\mathcal{L}_1}\int_{\mathcal{L}_2}\int_{\mathcal{L}_3}\mathsf{K}(s_1,s_2,s_3)ds_1ds_2\,ds_3\\ &= \frac{-1}{(2\pi w)^2}\int_{\mathcal{L}_2}\int_{\mathcal{L}_3}\mathrm{Res}[\mathsf{K}(s_1,s_2,s_3),s_1=\xi_1]ds_2ds_3.\end{aligned} \tag{31}$$

Using the residue theorem, $\mathrm{Res}[\mathsf{K}(s_1,s_2,s_3),s_1=\xi_1=\alpha_1\mu_1]$ can be developed as follows

$$\begin{aligned}&\mathrm{Res}[\mathsf{K}(s_1,s_2,s_3),\xi_1]\\ &= \lim_{s_1\to\xi_1}(s_1-\xi_1)\mathsf{K}(\xi_1,s_2,s_3)\\ &= -\alpha_1\Gamma(\alpha_1\mu_1)\left(\frac{\mathcal{C}_{1,1}}{\sqrt{\bar{\gamma}}}\right)^{\alpha_1\mu_1}\frac{\Gamma\left(A-\frac{\alpha_1\mu_1+s_2+s_3}{2}\right)}{\Gamma(\alpha_1\mu_1+s_2+s_3)}\\ &\quad\times\Gamma\left(\frac{\alpha_1\mu_1+s_2+s_3}{2}\right)\phi(s_2)\phi(s_3)\left(\frac{\mathcal{C}_{1,2}}{\sqrt{\bar{\gamma}}}\right)^{s_2}\left(\frac{\mathcal{C}_{1,3}}{\sqrt{\bar{\gamma}}}\right)^{s_3}.\end{aligned} \tag{32}$$

Next, substituting (32) into (31), we have

$$\begin{aligned}\Delta \approx\ &\frac{\alpha_1\Gamma(\alpha_1\mu_1)}{(2\pi w)^2}\left(\frac{\mathcal{C}_{1,1}}{\sqrt{\bar{\gamma}}}\right)^{\alpha_1\mu_1}\int_{\mathcal{L}_2}\int_{\mathcal{L}_3}\frac{\Gamma\left(A-\frac{\alpha_1\mu_1+s_2+s_3}{2}\right)}{\Gamma(\alpha_1\mu_1+s_2+s_3)}\\ &\times\Gamma\left(\frac{\alpha_1\mu_1+s_2+s_3}{2}\right)\phi(s_2)\phi(s_3)\left(\frac{\mathcal{C}_{1,2}}{\sqrt{\bar{\gamma}}}\right)^{s_2}\\ &\times\left(\frac{\mathcal{C}_{1,3}}{\sqrt{\bar{\gamma}}}\right)^{s_3}ds_2ds_3.\end{aligned} \tag{33}$$

In continuation with the asymptotic analysis, the integrals over $\mathcal{L}_2$ and $\mathcal{L}_3$ are similarly evaluated at the residue points $\xi_2=\alpha_2\mu_2$ and $\xi_3=\alpha_3\mu_3$, respectively. Next applying the residue theorem, the proof for (20) is finished.

$$\begin{aligned}\mathcal{U} &= \frac{\eta_M}{2\Gamma(A)}\int_0^\infty H_{1,1}^{1,1}\left[\gamma\,\middle|\,\begin{matrix}(1-A,1)\\(0,1)\end{matrix}\right]\frac{1}{(2\pi w)^M}\int_{\mathcal{L}_1}\cdots\int_{\mathcal{L}_M}\Phi(s_1,\cdots,s_M)\prod_{j=1}^{M}\frac{\mathcal{C}_j^{s_j}\phi(s_j)}{\sqrt{\bar{\gamma}\gamma}}\left(\sqrt{\frac{\gamma}{\bar{\gamma}}}\right)^{s_j-1}ds_1,\cdots,ds_Md\gamma\\ &\overset{(d)}{=} \frac{\eta_M(2\pi w)^{-M}}{2\Gamma(A)}\int_{\mathcal{L}_1}\cdots\int_{\mathcal{L}_M}\Phi(s_1,\cdots,s_M)\prod_{j=1}^{M}\phi(s_j)\left(\frac{\mathcal{C}_j}{\sqrt{\bar{\gamma}}}\right)^{s_j}\underbrace{\int_0^\infty\gamma^{\sum_{j=1}^{M}\frac{s_j}{2}-1}H_{1,1}^{1,1}\left[\gamma\,\middle|\,\begin{matrix}(1-A,1)\\(0,1)\end{matrix}\right]d\gamma}_{\mathcal{U}_1}ds_1,\cdots,ds_M\end{aligned} \tag{28}$$

When $N = 1$, then $\xi_j = \alpha_j \mu_j$, each single Mellin-Barnes integral is expanded at ξ_j, i.e.,

$$\text{Res}\left[\phi(s_j)\left(\frac{\mathcal{C}_{1,j}}{\sqrt{\bar{\gamma}}}\right)^{s_j}, \xi_j\right] = \lim_{s_j \to \xi_j} (s_j - \xi_j)\phi(s_j)\left(\frac{\mathcal{C}_{1,j}}{\sqrt{\bar{\gamma}}}\right)^{s_j},$$

subsequently, following the steps for (20), the proof for (21) is obtained.

REFERENCES

[1] D. Wu and R. Negi, "Effective capacity: A wireless link model for support of quality of service," *IEEE Trans. Wireless Commun.*, vol. 24, no. 5, pp. 630–643, May 2003.

[2] M. C. Gursoy, "MIMO wireless communications under statistical queueing constraints," *IEEE Trans. Inf. Theory*, vol. 57, no. 9, pp. 5897–5917, Sep. 2011.

[3] M. Amjad, L. Musavian, and M. H. Rehmani, "Effective capacity in wireless networks: A comprehensive survey," *IEEE Commun. Surveys Tuts.*, vol. 21, no. 4, pp. 3007–3038, 4th Quart., 2019.

[4] W. Yu, A. Chorti, L. Musavian, H. V. Poor, and Q. Ni, "Effective secrecy rate for a downlink NOMA network," *IEEE Trans. Wireless Commun.*, vol. 18, no. 12, pp. 5673–5690, Dec. 2019.

[5] V. Kumar, B. Cardiff, S. Prakriya, and M. F. Flanagan, "Delay violation probability and effective rate of downlink NOMA over α-μ fading channels," *IEEE Trans. Veh. Technol.*, vol. 69, no. 10, pp. 11241–11252, Oct. 2020.

[6] M. Amjad, L. Musavian, and S. Aïssa, "Effective capacity of NOMA with finite blocklength for low-latency communications," 2020, *arXiv:2002.07098*. [Online]. Available: http://arxiv.org/abs/2002.07098

[7] V. Kumar, B. Cardiff, S. Prakriya, and M. F. Flanagan, "Effective rate of downlink NOMA over K-μ shadowed fading with integer fading parameters," in *Proc. IEEE Int. Conf. Commun. Workshops (ICC Workshops)*, Dublin, Ireland, Jun. 2020, pp. 1–7.

[8] C. Guo, L. Liang, and G. Y. Li, "Resource allocation for low-latency vehicular communications: An effective capacity perspective," *IEEE J. Sel. Areas Commun.*, vol. 37, no. 4, pp. 905–917, Apr. 2019.

[9] M. You, H. Sun, J. Jiang, and J. Zhang, "Effective rate analysis in weibull fading channels," *IEEE Wireless Commun. Lett.*, vol. 5, no. 4, pp. 340–343, Aug. 2016.

[10] J. Zhang, L. Dai, Z. Wang, D. W. K. Ng, and W. H. Gerstacker, "Effective rate analysis of MISO systems over α-μ fading channels," in *Proc. IEEE GLOBECOM*, Dec. 2015, pp. 1–6.

[11] X. Li, J. Li, L. Li, J. Jin, J. Zhang, and D. Zhang, "Effective rate of MISO systems over κ–μ shadowed fading channels," *IEEE Access*, vol. 5, pp. 10605–10611, 2017.

[12] Z. Ji, C. Dong, Y. Wang, and J. Lu, "On the analysis of effective capacity over generalized fading channels," in *Proc. IEEE Int. Conf. Commun. (ICC)*, Jun. 2014, pp. 1977–1983.

[13] M. You, H. Sun, J. Jiang, and J. Zhang, "Unified framework for the effective rate analysis of wireless communication systems over MISO fading channels," *IEEE Trans. Commun.*, vol. 65, no. 4, pp. 1775–1785, Apr. 2017.

[14] F. S. Almehmadi and O. S. Badarneh, "On the effective capacity of Fisher–Snedecor $\mathcal{F}$ fading channels," *Electron. Lett.*, vol. 54, no. 18, pp. 1068–1070, Sep. 2018.

[15] H. Al-Hmood and H. S. Al-Raweshidy, "Unified approaches based effective capacity analysis over composite α-η-μ/gamma fading channels," *Electron. Lett.*, vol. 54, no. 13, pp. 852–853, Jun. 2018.

[16] H. Kaur, V. Kansal, and S. Singh, "Effective rate analysis of two-wave with diffuse-power fading channels," *IET Commun.*, vol. 13, no. 3, pp. 339–344, Feb. 2019.

[17] R. Singh, M. Rawat, and P. M. Pradhan, "Effective capacity of wireless networks over double shadowed rician fading channels," *Wireless Netw.*, vol. 26, no. 2, pp. 1347–1355, Feb. 2020.

[18] Y. Ai, A. Mathur, L. Kong, and M. Cheffena, "Effective throughput analysis of α-η-κ-μ fading channels," *IEEE Access*, vol. 8, pp. 57363–57371, 2020.

[19] H. Al-Hmood and H. Al-Raweshidy, "On the effective rate and energy detection based spectrum sensing over α–η–κ–μ fading channels," *IEEE Trans. Veh. Technol.*, vol. 69, no. 8, pp. 9112–9116, Aug. 2020.

[20] S. K. Yoo, S. L. Cotton, P. C. Sofotasios, S. Muhaidat, and G. K. Karagiannidis, "Effective capacity analysis over generalized composite fading channels," *IEEE Access*, vol. 8, pp. 123756–123764, 2020.

[21] C. Zhong, T. Ratnarajah, K.-K. Wong, and M.-S. Alouini, "Effective capacity of multiple antenna channels: Correlation and keyhole," *IET Commun.*, vol. 6, no. 12, pp. 1757–1768, Aug. 2012.

[22] I. Z. Kovacs, P. C. F. Eggers, K. Olesen, and L. G. Petersen, "Investigations of outdoor-to-indoor mobile-to-mobile radio communication channels," in *Proc. IEEE 56th Veh. Technol. Conf.*, vol. 1, Vancouver, BC, Canada, Sep. 2002, pp. 430–434.

[23] G. K. Karagiannidis, N. C. Sagias, and P. T. Mathiopoulos, "N^*Nakagami: A novel stochastic model for cascaded fading channels," *IEEE Trans. Commun.*, vol. 55, no. 8, pp. 1453–1458, Aug. 2007.

[24] L. Kong, G. Kaddoum, and D. B. da Costa, "Cascaded $\alpha - \mu$ fading channels: Reliability and security analysis," *IEEE Access*, vol. 6, pp. 41978–41992, 2018.

[25] O. S. Badarneh, S. Muhaidat, P. C. Sofotasios, S. L. Cotton, K. Rabie, and D. B. da Costa, "The N* Fisher-snedecor F cascaded fading model," in *Proc. 14th Int. Conf. Wireless Mobile Comput., Netw. Commun. (WiMob)*, Limassol, Cyprus, Oct. 2018, pp. 1–7.

[26] Z. Hadzi-Velkov, N. Zlatanov, and G. K. Karagiannidis, "Level crossing rate and average fade duration of the multihop Rayleigh fading channel," in *Proc. IEEE Int. Conf. Commun. (ICC)*, May 2008, pp. 4451–4455.

[27] L. Yang, F. Meng, Q. Wu, D. B. da Costa, and M.-S. Alouini, "Accurate closed-form approximations to channel distributions of RIS-aided wireless systems," *IEEE Wireless Commun. Lett.*, vol. 9, no. 11, pp. 1985–1989, Nov. 2020.

[28] M. Di Renzo, A. Zappone, M. Debbah, M.-S. Alouini, C. Yuen, J. de Rosny, and S. Tretyakov, "Smart radio environments empowered by reconfigurable intelligent surfaces: How it works, state of research, and the road ahead," *IEEE J. Sel. Areas Commun.*, vol. 38, no. 11, pp. 2450–2525, Nov. 2020.

[29] E. Basar, "Reconfigurable intelligent surface-based index modulation: A new beyond MIMO paradigm for 6G," *IEEE Trans. Commun.*, vol. 68, no. 5, pp. 3187–3196, May 2020.

[30] J. Zhang, E. Bjornson, M. Matthaiou, D. W. K. Ng, H. Yang, and D. J. Love, "Prospective multiple antenna technologies for beyond 5G," *IEEE J. Sel. Areas Commun.*, vol. 38, no. 8, pp. 1637–1660, Aug. 2020.

[31] M. D. Yacoub, "The α-μ distribution: A physical fading model for the Stacy distribution," *IEEE Trans. Veh. Technol.*, vol. 56, no. 1, pp. 27–34, Jan. 2007.

[32] A. K. Papazafeiropoulos and S. A. Kotsopoulos, "Generalized phase-crossing rate and random FM noise for α-μ fading channels," *IEEE Trans. Veh. Technol.*, vol. 59, no. 1, pp. 494–499, Jan. 2010.

[33] E. J. Leonardo and M. D. Yacoub, "Product of α-μ variates," *IEEE Wireless Commun. Lett.*, vol. 4, no. 6, pp. 637–640, Dec. 2015.

[34] U. S. Dias and M. D. Yacoub, "On the α-μ autocorrelation and power spectrum functions: Field trials and validation," in *Proc. IEEE GLOBECOM*, Honolulu, HI, USA, Nov. 2009, pp. 1–6.

[35] Q. Wu, D. W. Matolak, and I. Sen, "5-GHz-band vehicle-to-vehicle channels: Models for multiple values of channel bandwidth," *IEEE Trans. Veh. Technol.*, vol. 59, no. 5, pp. 2620–2625, Jun. 2010.

[36] P. Karadimas, E. D. Vagenas, and S. A. Kotsopoulos, "On the Scatterers' mobility and second order statistics of narrowband fixed outdoor wireless channels," *IEEE Trans. Wireless Commun.*, vol. 9, no. 7, pp. 2119–2124, Jul. 2010.

[37] P. K. Chong, S.-E. Yoo, S. H. Kim, and D. Kim, "Wind-blown foliage and human-induced fading in ground-surface narrowband communications at 400 MHz," *IEEE Trans. Veh. Technol.*, vol. 60, no. 4, pp. 1326–1336, May 2011.

[38] A. Michalopoulou, A. A. Alexandridis, K. Peppas, T. Zervos, F. Lazarakis, K. Dangakis, and D. I. Kaklamani, "Statistical analysis for on-body spatial diversity communications at 2.45 GHz," *IEEE Trans. Antennas Propag.*, vol. 60, no. 8, pp. 4014–4019, Aug. 2012.

[39] J. Reig and L. Rubio, "Estimation of the composite fast fading and shadowing distribution using the log-moments in wireless communications," *IEEE Trans. Wireless Commun.*, vol. 12, no. 8, pp. 3672–3681, Aug. 2013.

[40] D. Da Costa, M. Yacoub, and J. Filho, "Highly accurate closed-form approximations to the sum of α-μ variates and applications," *IEEE Trans. Wireless Commun.*, vol. 7, no. 9, pp. 3301–3306, Sep. 2008.

[41] D. Da Costa and M. Yacoub, "Accurate approximations to the sum of generalized random variables and applications in the performance analysis of diversity systems," *IEEE Trans. Commun.*, vol. 57, no. 5, pp. 1271–1274, May 2009.

[42] K. P. Peppas, "Sum of nonidentical squared $\kappa-\mu$ variates and applications in the performance analysis of diversity receivers," *IEEE Trans. Veh. Technol.*, vol. 61, no. 1, pp. 413–419, Jan. 2012.

[43] O. S. Badarneh, D. B. da Costa, P. C. Sofotasios, S. Muhaidat, and S. L. Cotton, "On the sum of Fisher–Snedecor $\mathcal{F}$ variates and its application to maximal-ratio combining," *IEEE Wireless Commun. Lett.*, vol. 7, no. 6, pp. 966–969, Dec. 2018.

[44] H. Du, J. Zhang, J. Cheng, and B. Ai, "Sum of Fisher-Snedecor $\mathcal{F}$ random variables and its applications," *IEEE Open J. Commun. Soc.*, vol. 1, pp. 342–356, 2020.

[45] P. Zhang, J. Zhang, K. P. Peppas, D. W. K. Ng, and B. Ai, "Dual-hop relaying communications over Fisher-Snedecor $\mathcal{F}$-fading channels," *IEEE Trans. Commun.*, vol. 68, no. 5, pp. 2695–2710, May 2020.

[46] J. Zheng, J. Zhang, G. Pan, J. Cheng, and B. Ai, "Sum of squared fluctuating two-ray random variables with wireless applications," *IEEE Trans. Veh. Technol.*, vol. 68, no. 8, pp. 8173–8177, Aug. 2019.

[47] Y. A. Rahama, M. H. Ismail, and M. S. Hassan, "On the sum of independent Fox's H-function variates with applications," *IEEE Trans. Veh. Technol.*, vol. 67, no. 8, pp. 6752–6760, Aug. 2018.

[48] A. M. Mathai, R. K. Saxena, and H. J. Haubold, *The H-Function: Theory and Applications*. New York, NY, USA: Springer-Verlag, 2009.

[49] L. Kong, G. Kaddoum, and H. Chergui, "On physical layer security over Fox's H-function wiretap fading channels," *IEEE Trans. Veh. Technol.*, vol. 68, no. 7, pp. 6608–6621, Jul. 2019.

[50] H. R. Alhennawi, M. M. H. El Ayadi, M. H. Ismail, and H.-A.-M. Mourad, "Closed-form exact and asymptotic expressions for the symbol error rate and capacity of the H-function fading channel," *IEEE Trans. Veh. Technol.*, vol. 65, no. 4, pp. 1957–1974, Apr. 2016.

[51] B. Selim, O. Alhussein, S. Muhaidat, G. K. Karagiannidis, and J. Liang, "Modeling and analysis of wireless channels via the mixture of Gaussian distribution," *IEEE Trans. Veh. Technol.*, vol. 65, no. 10, pp. 8309–8321, Oct. 2016.

[52] L. Kong, S. Chatzinotas, and B. Ottersten, "Unified framework for secrecy characteristics with mixture of Gaussian (MoG) distribution," *IEEE Wireless Commun. Lett.*, vol. 9, no. 10, pp. 1625–1628, Oct. 2020.

[53] J. Zhang, M. Matthaiou, G. K. Karagiannidis, and L. Dai, "On the multivariate gamma–gamma distribution with arbitrary correlation and applications in wireless communications," *IEEE Trans. Veh. Technol.*, vol. 65, no. 5, pp. 3834–3840, May 2016.

[54] L. Yang, Y. Yang, M. O. Hasna, and M.-S. Alouini, "Coverage, probability of SNR gain, and DOR analysis of RIS-aided communication systems," *IEEE Wireless Commun. Lett.*, vol. 9, no. 8, pp. 1268–1272, Aug. 2020.

[55] E. Basar and I. Yildirim, "Indoor and outdoor physical channel modeling and efficient positioning for reconfigurable intelligent surfaces in mmWave bands," 2020, *arXiv:2006.02240*. [Online]. Available: http://arxiv.org/abs/2006.02240

[56] S. W. H. Shah, M. M. U. Rahman, A. N. Mian, A. Imran, S. Mumtaz, and O. A. Dobre, "On the impact of mode selection on effective capacity of device-to-device communication," *IEEE Wireless Commun. Lett.*, vol. 8, no. 3, pp. 945–948, Jun. 2019.

[57] A. P. Prudnikov, Y. A. Brychkov, and O. I. Marichev, *Integrals and Series: More Special Functions*, vol. 3. New York, NY, USA: Gordon and Breach Science, 1990.

[58] A. A. Kilbas, *H-Transforms: Theory and Applications. Analytical Methods and Special Functions*. Boca Raton, FL, USA: CRC Press, 2004.

[59] H. Chergui, M. Benjillali, and S. Saoudi, "Performance analysis of project-and-forward relaying in mixed MIMO-pinhole and Rayleigh dual-hop channel," *IEEE Commun. Lett.*, vol. 20, no. 3, pp. 610–613, Mar. 2016.

[60] L. Kong, G. Kaddoum, and Z. Rezki, "Highly accurate and asymptotic analysis on the SOP over SIMO α–μ fading channels," *IEEE Commun. Lett.*, vol. 22, no. 10, pp. 2088–2091, Oct. 2018.

[61] G. Pan, C. Tang, X. Zhang, T. Li, Y. Weng, and Y. Chen, "Physical-layer security over non-small-scale fading channels," *IEEE Trans. Veh. Technol.*, vol. 65, no. 3, pp. 1326–1339, Mar. 2016.

[62] J. M. Holtzman, "A simple, accurate method to calculate spread-spectrum multiple-access error probabilities," *IEEE Trans. Commun.*, vol. 40, no. 3, pp. 461–464, Mar. 1992.

[63] P. Brodtkorb, P. Johannesson, G. Lindgren, I. Rychlik, J. Rydén, and E. Sjö, "WAFO—A MATLAB toolbox for the analysis of random waves and loads," in *Proc. 10th Int. Offshore Polar Eng. Conf. (ISOPE)*, Seattle, WA, USA, vol. 3, 2000, pp. 343–350.

[64] H. Chergui, M. Benjillali, and M.-S. Alouini, "Rician K-factor-based analysis of XLOS service probability in 5G outdoor ultra-dense networks," *IEEE Wireless Commun. Lett.*, vol. 8, no. 2, pp. 428–431, Apr. 2019.

LONG KONG received the B.S. degree in telecommunication engineering from Hainan University, Haikou, Hainan, China, in 2010, the M.S. degree in communication engineering from Xiamen University, Xiamen, China, in 2013, and the Ph.D. degree from the École de Technologie Supérieure (ÉTS), Université du Québec, Montréal, QC, Canada. Since September 2019, he has been a Research Associate with the Interdisciplinary Center for Security, Reliability and Trust (SnT), University of Luxembourg, Luxembourg. From January 2019 to April 2019, he was an Exchange Student with the Center of Wireless Communications (CWC), University of Oulu, Oulu, Finland, supported by the Mitacs Globalink Program. From August 2013 to November 2014, he was a Research Assistant of electronic and information engineering (EIE) with The Hong Kong Polytechnic University, Hong Kong. His research interests include physical layer security, cooperative communications, and chaos-based communication systems.

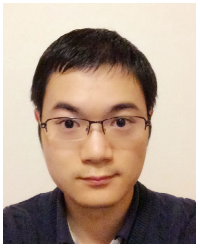

YUN AI (Member, IEEE) received the M.Sc. degree in electrical engineering from the Chalmers University of Technology, Göteborg, Sweden, in 2012, and the Ph.D. degree from the University of Oslo, Oslo, Norway, in 2018. In 2016, he was a Visiting Researcher with the Department of Information and Computer Science, Keio University, Tokyo, Japan. In 2016, funded by a stipend from the Norwegian University Center, Saint Petersburg, Russia, he was a Visiting Researcher with the Faculty of Applied Mathematics and Control Processes, Saint Petersburg State University, Saint Petersburg. He has been with the Signal Processing Group, Technische Universität Darmstadt, Darmstadt, Germany, as a Research Student and also with Ericsson as an Engineer. He is currently a Researcher with the Norwegian University of Science and Technology (NTNU), Norway. His current research interests include the broad areas of wireless communications with focuses on communication theory, wireless sensor networks, and smart grids.

SYMEON CHATZINOTAS (Senior Member, IEEE) received the M.Eng. degree in telecommunications from the Aristotle University of Thessaloniki, Thessaloniki, Greece, in 2003, and the M.Sc. and Ph.D. degrees in electronic engineering from the University of Surrey, Surrey, U.K., in 2006 and 2009, respectively.

He was a Visiting Professor with the University of Parma, Italy, and he was involved in numerous research and development projects with the National Center for Scientific Research Demokritos, the Center of Research and Technology Hellas, and the Center of Communication Systems Research, University of Surrey. He is currently a Full Professor/Chief Scientist I and the Co-Head of the SIGCOM Research Group with the SnT, University of Luxembourg. He has authored or coauthored more than 400 technical articles in refereed international journals, conferences, and scientific books. He was a co-recipient of the 2014 IEEE Distinguished Contributions to Satellite Communications Award, the CROWNCOM 2015 Best Paper Award, and the 2018 EURASIC JWCN Best Paper Award. He is also on the Editorial Board of the IEEE Open Journal of Vehicular Technology and the *International Journal of Satellite Communications and Networking*.

BJÖRN OTTERSTEN (Fellow, IEEE) was born in Stockholm, Sweden, in 1961. He received the M.S. degree in electrical engineering and applied physics from Linköping University, Linköping, Sweden, in 1986, and the Ph.D. degree in electrical engineering from Stanford University, Stanford, CA, USA, in 1990.

He has held research positions at the Department of Electrical Engineering, Linköping University, the Information Systems Laboratory, Stanford University, the Katholieke Universiteit Leuven, Leuven, Belgium, and the University of Luxembourg, Luxembourg. From 1996 to 1997, he was the Director of Research with ArrayComm, Inc., a start-up in San Jose, CA, USA, based on his patented technology. In 1991, he was appointed a Professor of signal processing with the Royal Institute of Technology (KTH), Stockholm. From 1992 to 2004, he was the Head of the Department for Signals, Sensors, and Systems, KTH, and from 2004 to 2008, he was the Dean of the School of Electrical Engineering, KTH. He is currently the Director for the Interdisciplinary Center for Security, Reliability and Trust, University of Luxembourg. As Digital Champion of Luxembourg, he acts as an Adviser to the European Commission. He is also a Fellow of EURASIP. He was a recipient of the IEEE Signal Processing Society Technical Achievement Award in 2011 and the European Research Council advanced research grant twice from 2009 to 2013 and since 2017. He has coauthored journal articles that received the IEEE Signal Processing Society Best Paper Award in 1993, 2001, 2006, and 2013, respectively, and seven other IEEE conference papers best paper awards. He has served as an Associate Editor for the IEEE TRANSACTIONS ON SIGNAL PROCESSING and the Editorial Board for the *IEEE Signal Processing Magazine*. He is also a member of the Editorial Boards of the *EURASIP Signal Processing Journal*, the *EURASIP Journal of Advances in Signal Processing*, and the *Foundations and Trends of Signal Processing*.